Chiral Bell-State Transfer via Dissipative Liouvillian Dynamics

Shishir Khandelwal,[1,2,3,*] Weijian Chen,[4] Kater W. Murch,[4] and Géraldine Haack[1]
[1]*Department of Applied Physics, University of Geneva, 1211 Geneva, Switzerland*
[2]*Physics Department, Lund University, Box 118, 22100 Lund, Sweden*
[3]*NanoLund, Lund University, Box 118, 22100 Lund, Sweden*
[4]*Department of Physics, Washington University, St. Louis, Missouri 63130, USA*

(Received 20 November 2023; accepted 6 June 2024; published 14 August 2024)

Chiral state transfer along closed loops in the vicinity of an exceptional point is one of the many counterintuitive observations in non-Hermitian physics. The application of this property beyond proof-of-principle in quantum physics, is an open question. In this work, we demonstrate chiral state conversion between singlet and triplet Bell states through fully quantum Liouvillian dynamics. Crucially, we demonstrate that this property can be used for the chiral production of Bell states from separable states with a high fidelity and for a large range of parameters. Additionally, we show that the removal of quantum jumps from the dynamics through postselection can result in near-perfect Bell states from initially separable states. Our work presents the first application of chiral state transfer in quantum information processing and demonstrates a novel way to control entangled states by means of dissipation engineering.

DOI: 10.1103/PhysRevLett.133.070403

Introduction—In recent years, exceptional points (EPs) in non-Hermitian systems have seen a surging interest, for example, in sensing [1–7], topological properties [8–14], and recently in the quantum control of dynamics [15–18]. Open quantum systems are a natural platform to explore EPs and associated effects as their evolution is characteristically non-Hermitian [19]. Chiral state transfer (CST) along closed trajectories in the vicinity of an EP is a well-known property of non-Hermitian physics, where eigenstates can be adiabatically switched, and the final state is solely determined by the orientation of the trajectories [20]. While this effect was first discussed for classical and semiclassical systems [21–26], its applications to quantum settings are only now being discovered. Theoretical works [27,28] have been accompanied by successful experiments with superconducting circuits [29,30] and single ions [31]. These results offer a pathway for quantum state control by utilizing dissipation as a resource. However, presently, they do not necessarily involve genuinely quantum phenomena, such as the creation of quantum correlations like entanglement, or offer an advantage in quantum settings.

In this work, we show for the first time, that it is possible to create highly entangled states by means of CST between two Bell states. We consider a minimal model of two interacting qubits, put in an out-of-equilibrium situation by coupling to thermal environments. This model has been used to demonstrate the presence of entanglement in the steady-state regime under autonomous dissipative dynamics only [32–36] and has recently been investigated in the context of EPs [15]. We demonstrate that slow trajectories in the parameter space of this system can result in CST between two Bell states. Importantly, this property can be utilized to create highly entangled states from arbitrary initial states. We further demonstrate that the transfer fidelity and entanglement can be increased by means of postselection, at the cost of reduced success rate [27,37]. Finally, we demonstrate that our results hold for a wide range of parameters, including trajectories not necessarily encircling EPs [12,26].

Model and trajectory in parameter space—We consider a system of interacting qubits, depicted in Fig. 1(a), with transition energies $\varepsilon_1 = \varepsilon$, $\varepsilon_2 = \varepsilon + \delta$. The full Hamiltonian takes the form $H_0 = \sum_{j=1,2} \varepsilon_j \sigma_+^{(j)} \sigma_-^{(j)} + g(\sigma_+^{(1)}\sigma_-^{(2)} + \sigma_-^{(1)}\sigma_+^{(2)})$ $(j = 1, 2)$, where $\sigma_\pm^{(j)}$ are the raising and lowering operators of qubit j and g is the interaction strength. Each qubit couples to its own fermionic environment with coupling strength γ_j. Under the assumption $g, \gamma_j, \delta \ll \varepsilon$, the Markovian evolution of the two qubits can be expressed in the following Lindblad form (with $\hbar = k_B = 1$) [38–40],

$$\dot{\rho} = \mathcal{L}\rho = -i[H_{\text{eff}}, \rho]_\dagger + \sum_{j=1,2} \gamma_j^+ \mathcal{J}_+^{(j)}\rho + \gamma_j^- \mathcal{J}_-^{(j)}\rho, \quad (1)$$

where $[a, b]_\dagger \coloneqq ab - b^\dagger a^\dagger$ and the effective non-Hermitian Hamiltonian (NHH) $H_{\text{eff}} \coloneqq H_0 - (i/2)\sum_j \gamma_j^- \sigma_+^{(j)}\sigma_-^{(j)} + \gamma_j^+ \sigma_-^{(j)}\sigma_+^{(j)}$. The superoperators $\mathcal{J}_\pm^{(j)}\rho \coloneqq \sigma_\pm^{(j)}\rho\sigma_\mp^{(j)}$ represent

*Contact author: shishir.khandelwal@teorfys.lu.se

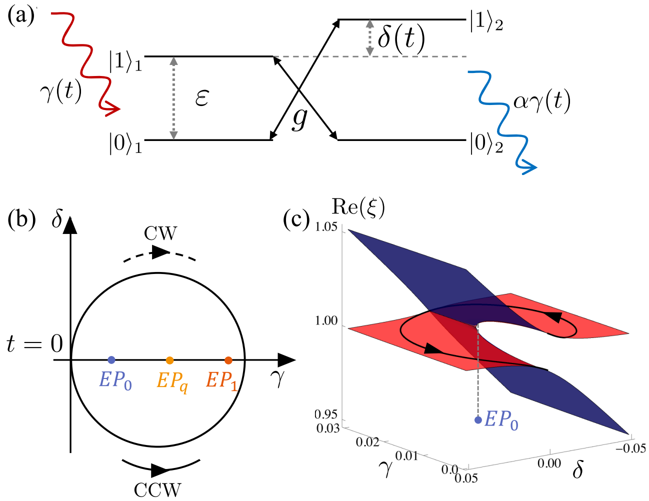

FIG. 1. (a) Two interacting qubits subject to gain and loss. (b) CW and CCW trajectories in the space of δ and γ, and depictions of EPs for different levels of postselection of quantum jumps, $q = 0$ (complete postselection), $q = 1$ (no postselection), and $0 < q < 1$ (partial postselection). (c) Riemann sheets corresponding to the NHH eigenvalues involved in the EP and a CCW trajectory showing state transfer. The more decaying branch of the eigenvalues (i.e., with more negative imaginary part) is depicted in red.

quantum jump terms. The corresponding excitation and deexcitation rates $\gamma_j^+ = \gamma_j n_j$ and $\gamma_j^- = \gamma_j(1 - n_j)$ are determined by the Fermi-Dirac distribution, $n_j = (e^{\beta_j(\varepsilon_1+\varepsilon_2)/2} + 1)^{-1}$ with inverse temperature β_j of reservoir j. We refer to these rates as "gain" and "loss," respectively. The NHH induces coherent nonunitary loss, while quantum jumps represent continuous monitoring by the environment [41]. It is possible to interpolate between purely NHH and fully quantum dynamics by using a hybrid-Liouvillian framework [37], with a quantum jump parameter, $q \in [0, 1]$,

$$\mathcal{L}_{[q]}\rho = -i[H_{\mathrm{eff}}, \rho]_{\dagger} + q \sum_{j=1,2} \gamma_j^+ \mathcal{J}_+^{(j)}\rho + \gamma_j^- \mathcal{J}_-^{(j)}\rho. \quad (2)$$

The case $q = 1$ corresponds to full Lindblad dynamics, $0 < q < 1$ to partial postselection and $q = 0$ to complete postselection. The spectra of H_{eff} and $\mathcal{L}_{[q]}$ and corresponding EPs are discussed in the Supplemental Material [42], Secs. I and II. Importantly, the NHH has a second-order EP involving eigenvectors which become Bell states $|\Psi^\pm\rangle = (|10\rangle \pm |01\rangle)/\sqrt{2}$ when the system is decoupled from the reservoirs (conversely, the eigenvectors $|\Psi^\pm\rangle$ of H_0 are involved in an EP in the presence of dissipation). By judicious choice of a parameter trajectory, it is expected that these Bell states play a central role in CST. This property is demonstrated on the Riemann sheets corresponding to the eigenvalues of H_{eff} depicted in Fig. 1(c), and forms the basis of the upcoming analysis.

We set $\gamma_1 := \gamma$ and $\gamma_2 := \alpha\gamma_1$ with $\alpha = \gamma_2/\gamma_1$ and choose a closed trajectory in the space of γ and δ [Fig. 1(b)]. We pick the following form of periodic driving of the parameters:

$$\delta(t) = \pm\Delta\delta \sin\left(\frac{2\pi t}{T}\right), \qquad \gamma(t) = \gamma_0 + \Delta\gamma \sin^2\left(\frac{\pi t}{T}\right), \quad (3)$$

where γ_0 sets the origin, $\Delta\delta$ and $\Delta\gamma$ are the amplitudes for $\delta(t)$, $\gamma(t)$ respectively, and T is the driving period. The "+" and "−" signs correspond to clockwise (CW) and counterclockwise (CCW) trajectories, respectively. By taking an appropriately large $\Delta\gamma$, the trajectory can be made to encircle the EPs. For any degree of postselection, $0 \leq q \leq 1$, the un-normalized state evolves according to $\rho(t) = \mathcal{T} \exp\left[\int_0^t \mathcal{L}_{[q]}(t')dt'\right]\rho(0)$, where $\mathcal{T}$ denotes time ordering. However, for $0 \leq q < 1$, the dynamics are not trace preserving. The following numerical results for $0 \leq q < 1$ have been calculated by discretizing the above time-ordered exponential and numerically renormalizing the state at every time step.

Chiral Bell-state transfer—We now turn to the core of this Letter: CST in the vicinity of EPs. We first investigate the case $\gamma_0 = 0$, in which the initial and final points (i.e., $t = 0$ and $t = T$) of the trajectory are $\gamma = \delta = 0$. In this case, at the initial and final points of the trajectory, H_0 and H_{eff} have the same spectrum and eigenvectors, $\{|11\rangle, |\Psi^+\rangle, |\Psi^-\rangle, |00\rangle\}$. Moreover, at $t = 0$, the eigenmatrices of $\mathcal{L}$ can be constructed from the eigenvectors of H_0 and H_{eff} [19]. This equivalence between Hamiltonian, NHH, and Liouvillian dynamics at the origin of the trajectory is essential for chiral Bell-state transfer. For a setup with fermionic reservoirs, we choose the inverse temperatures $\beta_1 \to -\infty$ and $\beta_2 \to \infty$. This corresponds to perfect population inversion in reservoir 1 ($n_1 = 1$) and to initialization in the lowest energy level ($n_2 = 0$) for reservoir 2, leading to the gain and loss situation shown in Fig. 1(a). As we will see later, this corresponds to the optimal setup for chiral Bell-state transfer. It also has a connection to parity-time symmetry in the setup (see the Supplemental Material [42], Sec. IV, and Ref. [43]). We characterize the state along the trajectory with its fidelity with respect to one of the Bell states, $\mathcal{F}_{|\Psi^\pm\rangle}(t) := \mathrm{Tr}\{|\Psi^\pm\rangle\langle\Psi^\pm|\rho(t)\}$.

When $q = 0$, H_{eff} dictates the dynamics, and CST is expected with near-perfect fidelity due to the conservation of purity (see the Supplemental Material [42], Sec. III). At the origin of the trajectory, the two states involved in the EP are $|\Psi^\pm\rangle$. Starting in $|\Psi^+\rangle$, the system either switches to $|\Psi^-\rangle$ or ends up again in $|\Psi^+\rangle$, depending on the orientation of the trajectory. In Fig. 2(a) (blue curves), we show this effect starting with $|\Psi^+\rangle$, which ends up at time $t = T$ nearly perfectly in the $|\Psi^-\rangle$ state for a CCW trajectory (solid) or comes back to $|\Psi^+\rangle$ for a CW trajectory (dashed). Therefore, switching between the states is chiral in nature.

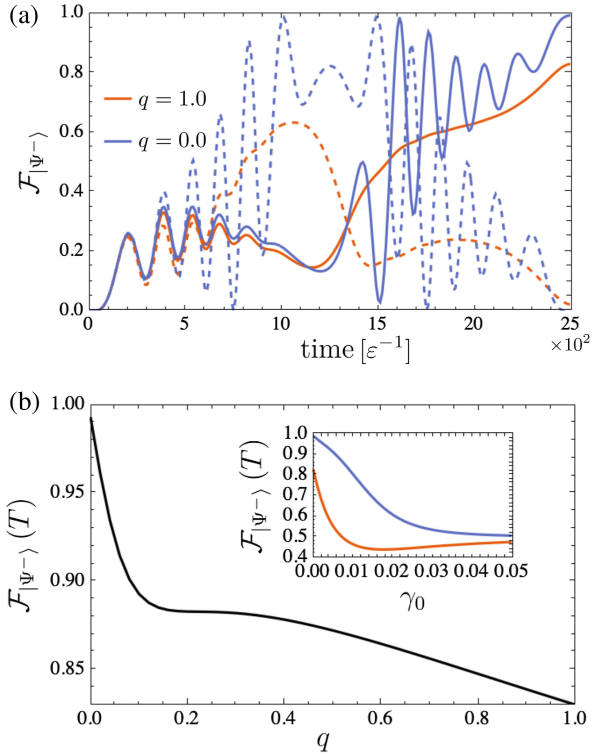

FIG. 2. (a) Fidelity of $\rho(t)$ with the Bell state $|\Psi^-\rangle$ as a function of time, for CW (dashed) and CCW (solid) trajectories. (b) The final fidelity (at time T) as a function of the quantum jump parameter q, shown only for the CCW trajectory. The inset shows the fidelity as a function of γ_0, which sets the origin of the trajectory, for $q = 0$ (blue) and $q = 1$ (red). The parameters are $\varepsilon = 1$, $\Delta\delta/\varepsilon = 0.04$, $\gamma_0 = 0$, $\Delta\gamma/\varepsilon = 0.008$, $g/\varepsilon = 0.01$, $\alpha = 1.2$, $\beta_1 \to -\infty$, $\beta_2 \to \infty$, and $T\varepsilon = 2500$.

As shown in the Supplemental Material [42], Sec. V, for $q = 0$, we find that maximal transfer fidelity can be achieved simply by taking sufficiently slow trajectories, i.e., CST is an adiabatic property.

Without complete postselection ($q \neq 0$), maximal transfer fidelity cannot be reached as Liouvillian dynamics do not preserve purity [44]. The case $q = 1$, which corresponds to full Liouvillian dynamics, is shown in red in Fig. 2(a) reaching a final fidelity $\mathcal{F}_{|\Psi^-\rangle} = 0.83$. We note that this is not an upper bound, and a higher fidelity can be achieved by suitably altering the parameters. The chirality of the state $|\Psi^-\rangle$ can similarly be verified; switching to $|\Psi^+\rangle$ is observed for a CW trajectory, while the state returns to $|\Psi^-\rangle$ for a CCW one, with the transfer fidelity remaining the same. In Fig. 2(b), we show that there is a monotonic decrease in transfer fidelity with increasing q (decreasing postselection). This corresponds to recent observations [27,29] and can be traced to the loss of purity with quantum jumps. Crucially, the inset in Fig. 2(b) shows a drastic fidelity loss for trajectories with origins far from $\gamma_0 = 0$. When the trajectory origin is chosen away from $\gamma_0 = 0$, Bell states are not the eigenstates of the NHH at the start and end of the trajectory. This means that state transfer occurs between some other states, which may be far from Bell states. This highlights the importance of the spectra of H_0, H_{eff}, and $\mathcal{L}$ being equivalent at the origin. Our analysis shows that CST is a property of the eigenstates of H_{eff}. While $\mathcal{L}_{[q]}$ (for $0 < q \leq 1$) shows it to a large extent, the fidelity is lowered due to loss of purity induced by quantum jumps.

For $q = 1$, the behavior can be analytically understood through the spectrum of the one-cycle evolution superoperator $\mathcal{P}(T) = \mathcal{T}\exp\left[\int_0^T \mathcal{L}(t')dt'\right]$ [45]. It has eigenvalues which either are 1 or lie within the unit circle. For long driving time periods T, the fixed point of the superoperator is reached, which corresponds to the unique eigenmatrix with eigenvalue 1. In the time-independent case, this eigenmatrix with eigenvalue 1 is equivalent to the eigenmatrix with eigenvalue 0 of the time-independent Liouvillian $\mathcal{L}$, corresponding to the usual steady state. This fixed point is independent of the initial state and only depends on the system and driving parameters. This can be understood within the framework of Floquet theory [45,46], which can also be useful to look at in the general case, $q \in [0, 1]$, with a corresponding $\mathcal{P}_{[q]}(T)$. While slow trajectories (i.e., with large T) are required for higher fidelities (see the Supplemental Material [42], Sec. V), adiabatic trajectories will drive the system to its instantaneous steady state at every point in the trajectory. Driving too slow may also lead to a loss of chirality [28]. We expect further insights may come from slow-driving perturbation theory, by calculating corrections to adiabatic evolution [47].

We now extend our predictions to the case where transport is not unidirectional, i.e., without perfect control of dissipation. We let $\beta_2 \to \infty$, implying perfect loss at qubit two, and calculate the final fidelity as a function of β_1 ($\beta_1 < 0$ implying population inversion). The absence of complete population inversion induces a decrease in the fidelity as shown in Fig. 3(a). Optimal fidelity is achieved for perfect population inversion, $\beta_1 \to -\infty$, independently of q. Moreover, for thermal environments ($\beta_1 > 0$), there is a drastic reduction in fidelity; the maximum is achieved for low β_1 ($\beta_1 \to 0$ or $n_1 \to 1/2$). Our analysis demonstrates that high transfer fidelity requires $n_1 > 1/2$, which corresponds to population inversion. It can further be verified that simultaneously, a low temperature for reservoir 2 is required for a high fidelity.

Finally, let us comment on the role of EPs in our predictions. It has recently been observed in some semiclassical settings that encircling EPs is not necessary for CST [25,26]. We find that encircling EPs in our setup is not necessary to achieve chiral Bell-state transfer. We illustrate this in Fig. 3(b) for different values of q, by varying the radius $\Delta\gamma$ of the trajectory along γ [see Eq. (3)]. The left side of each dashed line corresponds to trajectories not encircling the corresponding EP, while the right side corresponds to encircling trajectories. The plot showcases

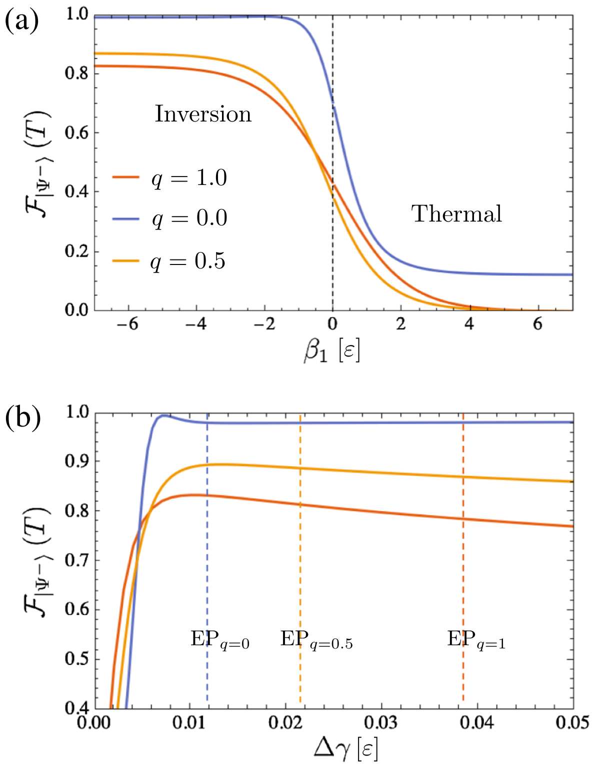

FIG. 3. (a) The final fidelity $\mathcal{F}_{|\Psi^-\rangle}(T)$ as a function of β_1, with $\beta_2 \to \infty$. (b) The final fidelity as a function of the amplitude $\Delta\gamma$. The trajectories are EP encircling on the right of each corresponding dashed line. The other parameters are taken from Fig. 2.

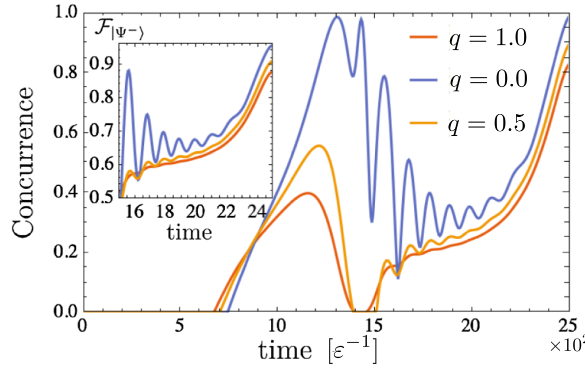

FIG. 4. Concurrence as a function of time with $\rho(0) = \mathbb{1}/4$, for various q. The inset shows the corresponding fidelity with $|\Psi^-\rangle$. The parameters are $\varepsilon = 1$, $\Delta\delta/\varepsilon = 0.06$, $\gamma_0 = 0$, $\Delta\gamma/\varepsilon = 0.01$, $g/\varepsilon = 0.01$, $\alpha = 1.2$, $\beta_1 \to -\infty$, $\beta_2 \to \infty$, and $T\varepsilon = 2500$. The trajectory is CCW.

the robustness of CST to changes in $\Delta\gamma$. Interestingly, we find that the maximum fidelity is obtained for trajectories not encircling the EPs. Whether there is a fundamental principle underlying this observation is an interesting question beyond the scope of this work.

Chiral production of Bell states—We now exploit chiral Bell-state transfer to demonstrate the generation of maximal two-qubit entanglement starting from any separable initial state. We consider the two qubits to be initially in a maximally mixed state, $\rho(0) = \mathbb{1}/4$, and take the same parameter driving as discussed above. Apart from the fidelity, we characterize the amount of entanglement through the concurrence $\mathcal{C}$ [48]. For density matrices ρ involved in our scheme, its expression simplifies to $\mathcal{C}(\rho) \coloneqq 2\max\{0, |c| - \sqrt{p_{11}p_{00}}\}$, with the populations $p_{11} = \langle 11|\rho|11\rangle$ and $p_{00} = \langle 00|\rho|00\rangle$, and coherence $c = \langle 01|\rho|10\rangle$; $\mathcal{C} = 0$ for a separable state, and $\mathcal{C} = 1$ for a maximally entangled state. In Fig. 4, the concurrence increases from 0 at $t = 0$, to its maximum at time $t = T$, where the system is driven close to the $|\Psi^-\rangle$ state. Importantly, for any q, a high concurrence can be obtained; specifically for $q = 1$, $\mathcal{C} > 0.83$. Although this is not an upper bound, it far exceeds the highest possible concurrence, $\mathcal{C}^{(\mathrm{aut})}_{\max} \approx 0.31$ [35,49], possible with the two-qubit system being operated autonomously (i.e., in the absence of driving or external control). Crucially, the production of Bell states has an associated chirality; for a CCW state, the system is driven to the $|\Psi^-\rangle$ state, while for a CW trajectory, to the $|\Psi^+\rangle$ state. Although the final state is independent of the initial state (for sufficiently large T), it is dependent on the parameters of the system. As the inset shows, a higher fidelity $\mathcal{F} \sim 0.9$ is obtained for the $q = 1$ case than in Fig. 2.

Experimental scope—We anticipate that an experimental implementation is readily achievable in the circuit QED platform [50], by utilizing a superconducting device consisting of two transmon circuits [51] that interact via a resonator-mediated coupling. The two transmons have individual readout resonators [52] that allow us to introduce the respective thermal baths. Positive and negative temperature fermionic baths can be replaced with engineered bosonic baths harnessing cavity assisted bath engineering [53], where population inversion can be achieved through off resonant driving of the qubit and associated cavity. Here, the qubit is driven with a detuning Δ and resonant Rabi frequency Ω_0. The cavity is driven with a detuning $\Delta' = \pm\sqrt{\Delta + \Omega_0}$. For positive (blue detuned) cavity drive, the qubit is pumped to the excited state, and the purity of the inversion is limited by the ratio of the cavity assisted bath engineering rate (ultimately limited by the cavity decay rate $\kappa = 1.3$ rad/μs), to the coherence times of the qubit. In this setup, coherence times are approximately $T_1, T_2^* \simeq 30$ μs. Hence we expect $n = 0.98$. The limit $q = 1$ (Lindblad dynamics) can be attained by harnessing the lowest two energy levels of the transmon [29,30], while $q = 0$ can be accessed by utilizing its higher manifold of states coupled with postselection [54]. Postselection, however, comes with the cost of reduced success probability for the protocol. The fidelity of the $q = 1$ limit can be deterministically improved by preventing transitions to the $|11\rangle$ state (see the Supplemental Material [42], Sec. VI). This can be achieved in a superconducting platform through the Zeno effect to decouple this state from the dynamics [55,56].

Discussion—We have theoretically demonstrated Liouvillian CST involving Bell states in a system of two dissipative qubits. This property allows for the chiral production of near-perfect Bell states starting with any separable initial state, breaking the bounds for autonomous dissipative entanglement production. The results hold for a large range of parameters, operating in the vicinity of an EP, without the necessity of encircling it.

Our results have implications beyond simple two-qubit models, and present a recipe for quantum state control through controlled dissipation and clever eigenstate engineering. For example, by judicious choice of many-qubit Hamiltonians and dissipation, our results suggest that CST, and by extension, entanglement production, can be seen for genuinely multipartite entangled states, like the W or GHZ state [57].

Acknowledgments—We thank Soumya S. Kumar for contributions to an early stage of this project and Parveen Kumar for useful correspondence. S. K. and G. H. acknowledge support from the SNSF through the starting grant PRIMA PR00P2_179748, as well as the NCCR SwissMAP for supporting short scientific visits. S. K. additionally acknowledges support from the Knut and Alice Wallenberg Foundation through the Wallenberg Center for Quantum Technology (WACQT). W. C. and K. M. acknowledge support from NSF Grant No. PHY-1752844 (CAREER), the Air Force Office of Scientific Research (AFOSR) Multidisciplinary University Research Initiative (MURI) Award on programmable systems with non-Hermitian quantum dynamics (Grant No. FA9550-21-1-0202), and ONR Grant No. N00014-21-1-2630.

[1] W. Chen, Ş. Kaya Özdemir, G. Zhao, J. Wiersig, and L. Yang, Nature (London) **548**, 192 (2017).
[2] M. Zhang, W. Sweeney, C. W. Hsu, L. Yang, A. Stone, and L. Jiang, Phys. Rev. Lett. **123**, 180501 (2019).
[3] S. Yu, Y. Meng, J.-S. Tang, X.-Y. Xu, Y.-T. Wang, P. Yin, Z.-J. Ke, W. Liu, Z.-P. Li, Y.-Z. Yang, G. Chen, Y.-J. Han, C.-F. Li, and G.-C. Guo, Phys. Rev. Lett. **125**, 240506 (2020).
[4] J. Wiersig, Photonics Res. **8**, 1457 (2020).
[5] M. D. Carlo, F. D. Leonardis, R. A. Soref, L. Colatorti, and V. M. N. Passaro, Sensors **22**, 3977 (2022).
[6] W. C. Wong and J. Li, New J. Phys. **25**, 033018 (2023).
[7] J. Larson and S. Qvarfort, Open Syst. Inf. Dyn. **30**, 2350008 (2023).
[8] A. A. Mailybaev, O. N. Kirillov, and A. P. Seyranian, Phys. Rev. A **72**, 014104 (2005).
[9] E. J. Bergholtz, J. C. Budich, and F. K. Kunst, Rev. Mod. Phys. **93**, 015005 (2021).
[10] K. Ding, C. Fang, and G. Ma, Nat. Rev. Phys. **4**, 745 (2022).
[11] W. Liu, Y. Wu, C.-K. Duan, X. Rong, and J. Du, Phys. Rev. Lett. **126**, 170506 (2021).
[12] M. Abbasi, W. Chen, M. Naghiloo, Y. N. Joglekar, and K. W. Murch, Phys. Rev. Lett. **128**, 160401 (2022).
[13] N. Okuma and M. Sato, Annu. Rev. Condens. Matter Phys. **14**, 83 (2023).
[14] I. I. Arkhipov, A. Miranowicz, F. Minganti, Ş. K. Özdemir, and F. Nori, Nat. Commun. **14**, 2076 (2023).
[15] S. Khandelwal, N. Brunner, and G. Haack, PRX Quantum **2**, 040346 (2021).
[16] P. Kumar, K. Snizhko, Y. Gefen, and B. Rosenow, Phys. Rev. A **105**, L010203 (2022).
[17] J.-W. Zhang, J.-Q. Zhang, G.-Y. Ding, J.-C. Li, J.-T. Bu, B. Wang, L.-L. Yan, S.-L. Su, L. Chen, F. Nori *et al.*, Nat. Commun. **13**, 6225 (2022).
[18] Y.-L. Zhou, X.-D. Yu, C.-W. Wu, X.-Q. Li, J. Zhang, W. Li, and P.-X. Chen, Phys. Rev. Res. **5**, 043036 (2023).
[19] F. Minganti, A. Miranowicz, R. W. Chhajlany, and F. Nori, Phys. Rev. A **100**, 062131 (2019).
[20] M. V. Berry and R. Uzdin, J. Phys. A **44**, 435303 (2011).
[21] C. Dembowski, B. Dietz, H.-D. Gräf, H. L. Harney, A. Heine, W. D. Heiss, and A. Richter, Phys. Rev. Lett. **90**, 034101 (2003).
[22] R. Uzdin, A. Mailybaev, and N. Moiseyev, J. Phys. A **44**, 435302 (2011).
[23] J. Doppler, A. A. Mailybaev, J. Böhm, U. Kuhl, A. Girschik, F. Libisch, T. J. Milburn, P. Rabl, N. Moiseyev, and S. Rotter, Nature (London) **537**, 76 (2016).
[24] H. Xu, D. Mason, L. Jiang, and J. Harris, Nature (London) **537**, 80 (2016).
[25] A. U. Hassan, G. L. Galmiche, G. Harari, P. LiKamWa, M. Khajavikhan, M. Segev, and D. N. Christodoulides, Phys. Rev. A **96**, 052129 (2017).
[26] H. Nasari, G. Lopez-Galmiche, H. E. Lopez-Aviles, A. Schumer, A. U. Hassan, Q. Zhong, S. Rotter, P. LiKamWa, D. N. Christodoulides, and M. Khajavikhan, Nature (London) **605**, 256 (2022).
[27] P. Kumar, K. Snizhko, and Y. Gefen, Phys. Rev. A **104**, L050405 (2021).
[28] K. Sun and W. Yi, Phys. Rev. A **108**, 013302 (2023).
[29] W. Chen, M. Abbasi, Y. N. Joglekar, and K. W. Murch, Phys. Rev. Lett. **127**, 140504 (2021).
[30] W. Chen, M. Abbasi, B. Ha, S. Erdamar, Y. N. Joglekar, and K. W. Murch, Phys. Rev. Lett. **128**, 110402 (2022).
[31] J.-T. Bu, J.-Q. Zhang, G.-Y. Ding, J.-C. Li, J.-W. Zhang, B. Wang, W.-Q. Ding, W.-F. Yuan, L. Chen, i. m. c. K. Özdemir, F. Zhou, H. Jing, and M. Feng, Phys. Rev. Lett. **130**, 110402 (2023).
[32] J. B. Brask, G. Haack, N. Brunner, and M. Huber, New J. Phys. **17**, 113029 (2015).
[33] F. Tacchino, A. Auffèves, M. F. Santos, and D. Gerace, Phys. Rev. Lett. **120**, 063604 (2018).
[34] S. Khandelwal, N. Palazzo, N. Brunner, and G. Haack, New J. Phys. **22**, 073039 (2020).
[35] K. Prech, P. Johansson, E. Nyholm, G. T. Landi, C. Verdozzi, P. Samuelsson, and P. P. Potts, Phys. Rev. Res. **5**, 023155 (2023).

[36] S. Khandelwal, B. Annby-Andersson, G. F. Diotallevi, A. Wacker, and A. Tavakoli, arXiv:2401.01776.

[37] F. Minganti, A. Miranowicz, R. W. Chhajlany, I. I. Arkhipov, and F. Nori, Phys. Rev. A **101**, 062112 (2020).

[38] H.-P. Breuer and F. Petruccione, *The Theory of Open Quantum Systems* (Oxford University Press, Oxford, 2007).

[39] P. P. Hofer, M. Perarnau-Llobet, L. D. M. Miranda, G. Haack, R. Silva, J. B. Brask, and N. Brunner, New J. Phys. **19**, 123037 (2017).

[40] P. P. Potts, A. A. S. Kalaee, and A. Wacker, New J. Phys. **23**, 123013 (2021).

[41] H. M. Wiseman and G. J. Milburn, *Quantum Measurement and Control* (Cambridge University Press, Cambridge, England, 2009), 10.1017/CBO9780511813948.

[42] See Supplemental Material at http://link.aps.org/supplemental/10.1103/PhysRevLett.133.070403 for the Liouvillian spectrum, discussion on properties such as the purity and parity-time symmetry and additional calculations on chiral state transfer.

[43] J. Huber, P. Kirton, S. Rotter, and P. Rabl, SciPost Phys. **9**, 052 (2020).

[44] A. Sergi and K. G. Zloshchastiev, Int. J. Mod. Phys. B **27**, 1350163 (2013).

[45] M. Hartmann, D. Poletti, M. Ivanchenko, S. Denisov, and P. Hänggi, New J. Phys. **19**, 083011 (2017).

[46] A. Schnell, A. Eckardt, and S. Denisov, Phys. Rev. B **101**, 100301 (2020).

[47] V. Cavina, A. Mari, and V. Giovannetti, Phys. Rev. Lett. **119**, 050601 (2017).

[48] W. K. Wootters, Phys. Rev. Lett. **80**, 2245 (1998).

[49] J. Bohr Brask, F. Clivaz, G. Haack, and A. Tavakoli, Quantum **6**, 672 (2022).

[50] A. Blais, A. L. Grimsmo, S. M. Girvin, and A. Wallraff, Rev. Mod. Phys. **93**, 025005 (2021).

[51] J. Koch, T. M. Yu, J. Gambetta, A. A. Houck, D. I. Schuster, J. Majer, A. Blais, M. H. Devoret, S. M. Girvin, and R. J. Schoelkopf, Phys. Rev. A **76**, 042319 (2007).

[52] C. Gaikwad, D. Kowsari, C. Brame, X. Song, H. Zhang, M. Esposito, A. Ranadive, G. Cappelli, N. Roch, E. M. Levenson-Falk, and K. W. Murch, Phys. Rev. Lett. **132**, 200401 (2024).

[53] K. W. Murch, U. Vool, D. Zhou, S. J. Weber, S. M. Girvin, and I. Siddiqi, Phys. Rev. Lett. **109**, 183602 (2012).

[54] M. Naghiloo, M. Abbasi, Y. N. Joglekar, and K. W. Murch, Nat. Phys. **15**, 1232 (2019).

[55] P. M. Harrington, E. J. Mueller, and K. W. Murch, Nat. Rev. Phys. **4**, 660 (2022).

[56] E. Blumenthal, C. Mor, A. A. Diringer, L. S. Martin, P. Lewalle, D. Burgarth, K. B. Whaley, and S. Hacohen-Gourgy, npj Quantum Inf. **8**, 88 (2022).

[57] W. Dür, G. Vidal, and J. I. Cirac, Phys. Rev. A **62**, 062314 (2000).